Distributed power and control actuation in the thoracic mechanics of a robotic insect

2010 Bioinspir. Biomim. 5 045006

(http://iopscience.iop.org/1748-3190/5/4/045006)

Bioinsp. Biomim. **5** (2010) 045006 (12pp) doi:10.1088/1748-3182/5/4/045006

Distributed power and control actuation in the thoracic mechanics of a robotic insect

Benjamin M Finio and Robert J Wood

Harvard University School of Engineering and Applied Sciences, Cambridge, MA 02138, USA

E-mail: bfinio@fas.harvard.edu

Received 6 April 2010
Accepted for publication 10 June 2010
Published 24 November 2010
Online at stacks.iop.org/BB/5/045006

Abstract
Recent advances in the understanding of biological flight have inspired roboticists to create flapping-wing vehicles on the scale of insects and small birds. While our understanding of the wing kinematics, flight musculature and neuromotor control systems of insects has expanded, in practice it has proven quite difficult to construct an at-scale mechanical device capable of similar flight performance. One of the key challenges is the development of an effective and efficient transmission mechanism to control wing motions. Here we present multiple insect-scale robotic thorax designs capable of producing asymmetric wing kinematics similar to those observed in nature and utilized by dipteran insects to maneuver. Inspired by the thoracic mechanics of dipteran insects, which entail a morphological separation of power and control muscles, these designs show that such distributed actuation can also modulate wing motion in a robotic design.

(Some figures in this article are in colour only in the electronic version)

1. Introduction

Extremely agile natural flyers such as insect orders Diptera and Hymenoptera have inspired engineers to create insect-sized, flapping-wing micro air vehicles (MAVs). Mechanical reproduction of this agile flight has proven challenging since technologies developed for flight at larger scales (e.g. airplanes and helicopters) fail to scale down appropriately to an insect-sized vehicle. Development of such vehicles requires the introduction of completely new fabrication techniques to allow production of insect-scale devices, as well as an intimate understanding of the internal (thoracic) and external (aerodynamic) mechanisms of insect flight. This has led engineers to work closely with biologists who study various aspects of insect flight dynamics in order to gain a better understanding of these mechanisms.

In hover, dipteran insects flap their wings while simultaneously rotating each wing about its longitudinal axis (figure 1). The wing motion is parameterized by three angles (figure 2), and asymmetric variations in these stroke parameters are the primary (but not only) method with which insects maneuver [1, 2].

One important discovery is that an insect thorax is a *resonant* structure [2]. Elasticity in the thorax means that large amounts of kinetic energy can be stored as potential energy and subsequently recovered on each stroke. For a mechanical structure, this means that an *oscillating* actuator may be more appropriate than a continuously rotating actuator such as a dc motor, which has no inherent potential energy storage. Since off-the-shelf dc motors are generally not available at the insect scale, an oscillatory actuator becomes even more appealing. Early attempts at creation of an insect-scale MAV such as the Berkeley micromechanical flying insect (MFI) [3] made use of oscillatory piezoelectric actuators. The Harvard microrobotic fly (HMF) [4–6] focused on the use of a harmonic actuator to flap wings at the system resonant frequency to increase efficiency. The HMF was capable of generating enough lift to achieve takeoff; however, the vehicle was tethered for stability, as it lacked the ability to generate asymmetric wing motions needed for stabilization and maneuvering. Here we present modifications to the original HMF design that allow

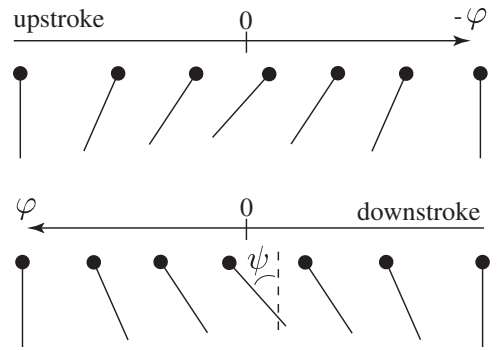

Figure 1. An edge-on view of an insect wing during the stroke. The black circle represents the leading edge of the wing; the line is a chordwise strip of the wing. The wing flaps back and forth in a nominally flat plane (vertical deviation from this plane is not depicted here) while simultaneously rotating about its longitudinal axis (which is parallel to, but not necessarily coincident with, the leading edge).

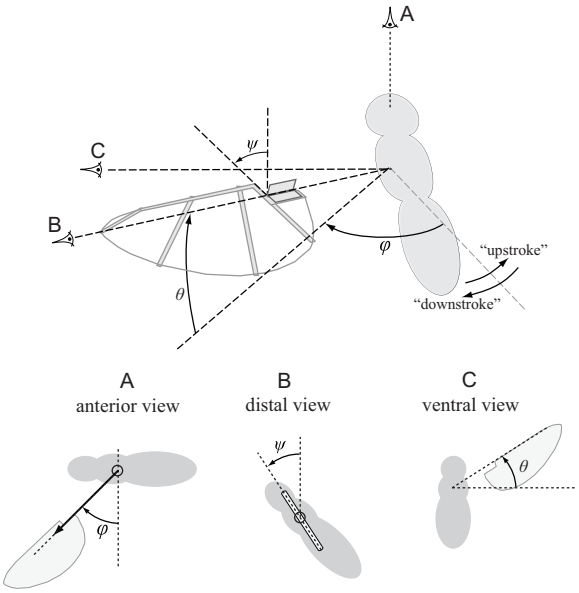

Figure 2. Definitions of the three wing angles: flapping angle ϕ, stroke plane deviation angle θ and rotation angle ψ.

asymmetric control of wing motion, as a first step toward the ultimate goal of an autonomous vehicle.

Two main questions arise when investigating the use of asymmetric wing kinematics for stability and control in insects: (1) which wing parameters need to be changed in order to maneuver or respond to a disturbance and (2) how are these motions generated? As engineers we are particularly interested in determining the minimum number of stroke parameters we must vary to obtain full control of the vehicle in three-dimensional space and the minimum number of actuators required to do so. The motivations are simple—on a vehicle with limited energy storage capacity, any unnecessary mechanism or actuator detracts from the useful payload or flight time. Again, we look to nature for a hint at the solution and find another important biological discovery, a key theme of this work: the separation of power and control muscles in insects. It has been known for some time that certain insect orders (e.g. Diptera, Hymenoptera and Coleoptera) possess two functionally and morphologically distinct groups of flight muscles [7] as opposed to more primitive orders where wing motion is controlled entirely by direct flight muscles [2, 8]. The power muscles are responsible for driving the wings at the resonant frequency of the thorax, but do so symmetrically, with nominally the same effect on each wing. The control muscles are used to 'fine-tune' wing motion, introducing bilateral asymmetries into the wingstroke, generating asymmetric aerodynamic forces on the wings, and thus a net body torque, resulting in the ability to maneuver. The use of control muscles to generate these asymmetric motions allows the power muscles to remain at or near their peak (most efficient) operating point.

Recent studies have examined the effects of individual sets of control muscles on wing kinematics [9–12] and on the wing kinematics insects use to make rapid turns [1]. Numerous kinematic parameters including but not limited to mean stroke angle, stroke plane inclination, angle of attack and stroke amplitude can be adjusted for maneuvering [11, 13] by at least 17 pairs of control muscles [9]. Rather than attempting to exactly replicate this system, we seek to introduce control over a sufficient number of parameters to allow controllability of a flying vehicle with six degrees of freedom (DOFs) in space with the primary goal of retaining separation of power and control actuators in order to allow the power actuator to remain at its peak operating efficiency. Particularly, from [1], we see that remarkably subtle asymmetric changes in stroke amplitude and stroke plane tilt are used by *Drosophila* to generate rapid turns (saccades) in the yaw direction. As a preliminary investigation into the use of distributed power and control actuation for flapping-wing MAVs, we present modifications to the original HMF design that include control actuators capable of introducing controlled asymmetries in stroke amplitude.

It should be noted that asymmetric wing kinematics are not the only method used by insects to maneuver or stabilize. Abdominal adjustments can be used to create an asymmetric body drag profile, and some insects will extend their legs to increase their rotational inertia in response to a gust of wind [14, 15]. At first it may seem that a more traditional approach to control, such as the use of flaps for thrust vectoring (equivalent to aelerons, elevators and rudders on an airplane), would be much simpler to implement. We choose to pursue asymmetric flapping-wing kinematics as a method of control for three reasons.

- Small vehicles are particularly vulnerable to wind gusts and disturbances—the addition of ancillary control surfaces will increase surface area and thus increase this vulnerability.
- Since aerodynamic forces are proportional to the square of velocity relative to the air, the forces available from a traditional mechanism such as a rudder will depend heavily on flight speed. In hover, the available control force will be reduced in magnitude since it will rely solely on downwash from the wings, and this will greatly reduce the vehicle's ability to maneuver at low speeds (analagous to why a helicopter has a tail rotor as opposed to a rudder). We also note that in nature, the use of a tail for thrust

vectoring is observed in larger flyers (e.g. birds) [16], but is generally not observed in hovering insects.

- On a small vehicle with limited payload capacity, any ancillary structure/actuator will detract from the useful payload. Therefore, using structures that are already in place (the wings) for control may be a weight-saving measure, as opposed to addition of separate control surfaces.

2. Mechanical design

2.1. Previous work

While some evidence suggests that insect wing rotation is largely passive [17], other studies have shown that some degree of control over wing rotation timing and angle of attack can be used to control maneuvers [11, 13, 18]. Mechanical reproduction of a device with direct control over both wing flapping and rotation has been attempted in previous flapping-wing MAV designs, which utilized separate power actuators to drive both flapping and rotation of each wing (with a flat stroke plane, i.e. $\theta \equiv 0$) [3, 19, 20], totalling four power actuators for four DOFs. For efficiency purposes (to minimize reactive power and amplify stroke amplitude), the system was designed to drive the wings at the resonant frequency of the flapping mode. However, this required matching the resonant frequency of the rotational mode to that of the flapping mode, and minimizing dynamic coupling between the two modes or also matching the resonant frequencies of the coupled motions. Any errors in this process—either in modeling the nonlinearities or fabrication of test devices—could lead to mismatched resonant frequencies and thus decreased efficiency.

The HMF introduced the simpler concept of using a single-power actuator to flap both wings, allowing wing rotation about the longitudinal axis to be passive. Each wing is attached to its driving link by a flexure hinge, allowing the wing to rotate passively due to inertial and aerodynamic forces while flapping. Thus the 3DOF structure only has one actuated DOF, introducing the trade-off of decreased controlled DOFs for greatly increased simplicity. This will make the control of a 6DOF body in space more difficult, especially since we do not expect any inherent passive stability (passive balancing of aerodynamic torques for the HMF is a parallel research area, see [21]). Some insects may benefit from pendulum stability as the body's center of mass 'hangs' below the wing base [13]. However, for the HMF, the stroke plane orientation is fixed with respect to the body, and therefore the net lift force (assuming symmetric wing motion) will always pass through the vehicle's center of mass. Therefore there will be no restoring torque to right the vehicle if it is perturbed from an upright orientation.

The HMF actuator is a piezoelectric bimorph [22], which provides an oscillating translational input to a symmetric fourbar transmission, which then drives two (symmetric) oscillating rotational outputs at the wings. Such actuators are appropriate for resonant actuation of flapping-wing devices since power density increases with increased operating frequencies (when operating the actuators quasi-statically); thus, for small systems with high resonant frequencies (hundreds of Hz), power densities rival those of dc motors. While such actuators may require high voltage drive signals (typically 200–300 V), milligram-scale power electronics are under development to allow the use of a conventional 3.7 V Li-polymer battery as a power supply [23]. The minimal design presented in [4–6], with all off-board electronics and no control actuators, has a mass of 60 mg and a 2:1 lift:weight ratio. Roughly 66% of this mass is the power actuator, compared to flight muscle ratios (relative to total body mass) ranging from roughly 20% to 50% in insects [24]. This leaves limited payload for control mechanics and additional onboard equipment such as power supplies and sensors ([25] presents an analysis of the energetics and mass budget of a flapping-wing MAV).

2.2. Thorax designs

Here we explore a sequence of methods to generate bilateral asymmetries while retaining the efficient thrust generation obtained from harmonic actuation and passive wing rotation. All three designs retain a single bimorph as a power actuator, but differ in their implementation of the control actuator(s).

(i) Two separate control actuators are mounted at the base of each wing. For a fixed sinusoidal power actuator input, each control actuator can be used to independently modulate the stroke amplitudes of the left and right wings. This design, initially presented in [26], is the most similar to the thoracic topology of a dipteran insect, where control muscles are directly connected at the base of the wing. See figure 3(*b*).

(ii) The power and control actuators are 'hybridized' into a 2DOF actuator consisting of one large bimorph to supply flapping power and a smaller bimorph to serve as a control input. Stroke amplitude can no longer be adjusted independently for the left and right wings—the single-control actuator couples amplitude changes between the two wings, i.e. the stroke amplitude of one wing cannot be decreased without simultaneously increasing the amplitude of the other wing. This design, initially presented in [27], removes the redundancy inherent in design 1. See figure 3(*c*).

(iii) The newest design also uses a 'hybrid' actuator but with a different actuator topology for control: a twisting unimorph (as opposed to bending bimorph) that provides a rotational input to the transmission. As with design 2, stroke amplitude changes are coupled between the two wings. The design and optimization of the twisting actuators themselves will be the subject of a future publication [28], but a brief discussion is presented here. Piezoelectric bimorph actuators contain two isotropic piezoelectric layers and a single orthotropic composite layer with carbon fibers running lengthwise along the actuator. Thus there is no asymmetry in material properties and pure bending can be achieved. If the actuator length is much greater than the output displacement, then the motion of the

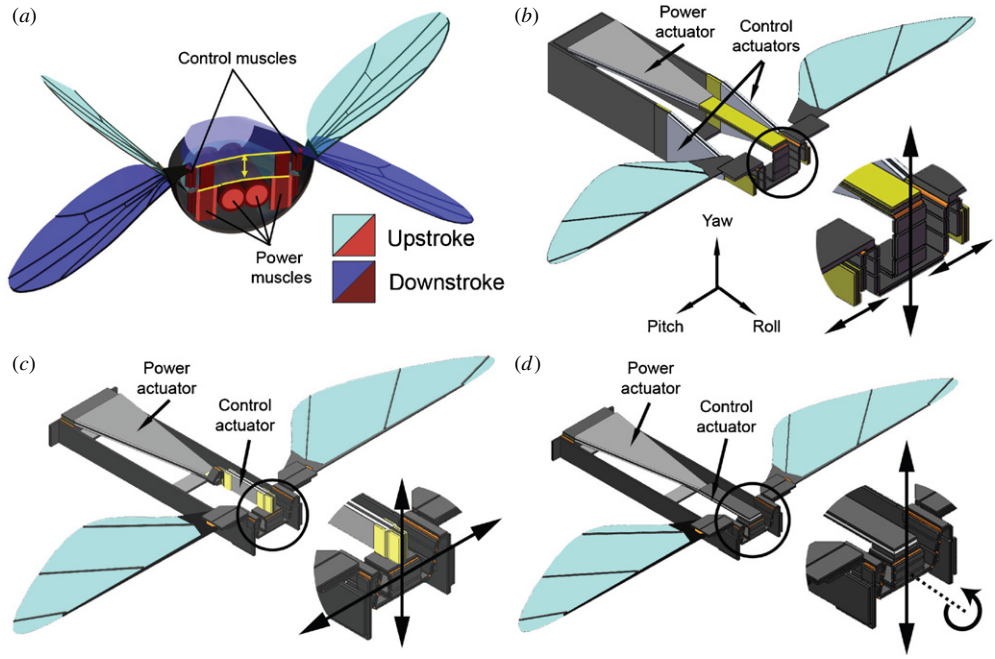

Figure 3. (*a*) Cross-sectional view of a dipteran insect thorax (artist's rendering, anatomical dimensions are not exact). The larger power muscles drive flapping motion through motion of the thorax but are not directly connected to the wings (the edge of the thorax that has been 'cut' by the cross-sectional view is highlighted, the upper line corresponds to the wings in the 'down' position and vice versa). Smaller control muscles at the base of the wings allow fine-tuning of the wingstroke parameters (ϕ, ψ and θ). Modulation of these parameters allows generation of net forces and body torques for maneuvering. (*b*) Our first design entails similar distribution of power and control actuation, where a large piezoelectric actuator drives wing flapping motion through a fourbar transmission structure, and smaller control actuators at the base of the wings allow asymmetric modulation of stroke amplitude. (*c*) Our second design hybridizes power and control into a single 2DOF actuator. (*d*) Our third design also uses a hybrid actuator, with a twisting (as opposed to bending) actuator for control. Details of each of these concepts are described in section 2.

tip can be approximated as linear and the actuator is modeled as a force source with translational output. The twisting actuators contain a single piezoelectric layer and two orthotropic composite layers with antisymmetric orientations, i.e. a top layer with fibers oriented at +45° relative to the longitudinal axis of the actuator, and a bottom layer at −45°. This antisymmetric layering creates asymmetries in the actuator's compliance matrix and allows exploitation of extension-twisting coupling effects, to create a rotational actuator with a torque output. These actuators can be analyzed using the same model presented in [22]. Energy densities are similar to bimorphs and thus they are also deemed suitable for flapping-wing MAV applications. The availability of a rotational, rather than a translational, input increases the number of possible transmission topologies, resulting in the third design presented here. See figure 3(*d*).

Each design can be analyzed such that wing motion can be predicted as a function of power and control actuator inputs. An overview of the kinematic and dynamic analysis is presented in the next section.

3. Kinematics and dynamics

3.1. Kinematics

A kinematic (i.e. purely geometric, taking no forces or inertias into account) analysis of the flapping mechanism can be undertaken using a pseudo-rigid body model as outlined in [29]. This approach treats carbon fiber spars as rigid links (i.e. infinitely stiff) and the flexure joints connecting them as ideal revolute joints in parallel with a torsional spring. This allows the flexure-based transmission mechanism, which converts linear actuator motion to wing rotation, to be analyzed as a pseudo-rigid body mechanism (figure 4). If all actuators are treated as pure displacement or pure rotation inputs, then actuator motion can be mapped directly to the wing stroke angle via an explicit geometric formulation. For the actuator inputs δ_i (or θ_i in the case of rotation) and transmission linkage geometry L_i (defined in figure 4), wing stroke angle ϕ is defined as follows:

$$\phi = \cos^{-1}\left(\frac{(L_y-\delta_1)^2+c_1}{c_2\sqrt{L_x^2+(L_y-\delta_1)^2}}\right)+\tan^{-1}\left(\frac{L_x}{L_y-\delta_1}\right) + \tan^{-1}\left(\frac{L_2-L_4}{L_3}\right)-\frac{\pi}{2} \tag{1}$$

where δ_1 is the power actuator input displacement and L_x, L_y, c_1 and c_2 are defined as

$$L_x = L_3 + \mathrm{d}x \tag{2}$$

$$L_y = L_1 + L_2 - L_4 + \mathrm{d}y \tag{3}$$

$$c_1 = L_3^2 + (L_2-L_4)^2 - L_1^2 - L_x^2 \tag{4}$$

$$c_2 = 2\sqrt{L_3^2+(L_2-L_4)^2} \tag{5}$$

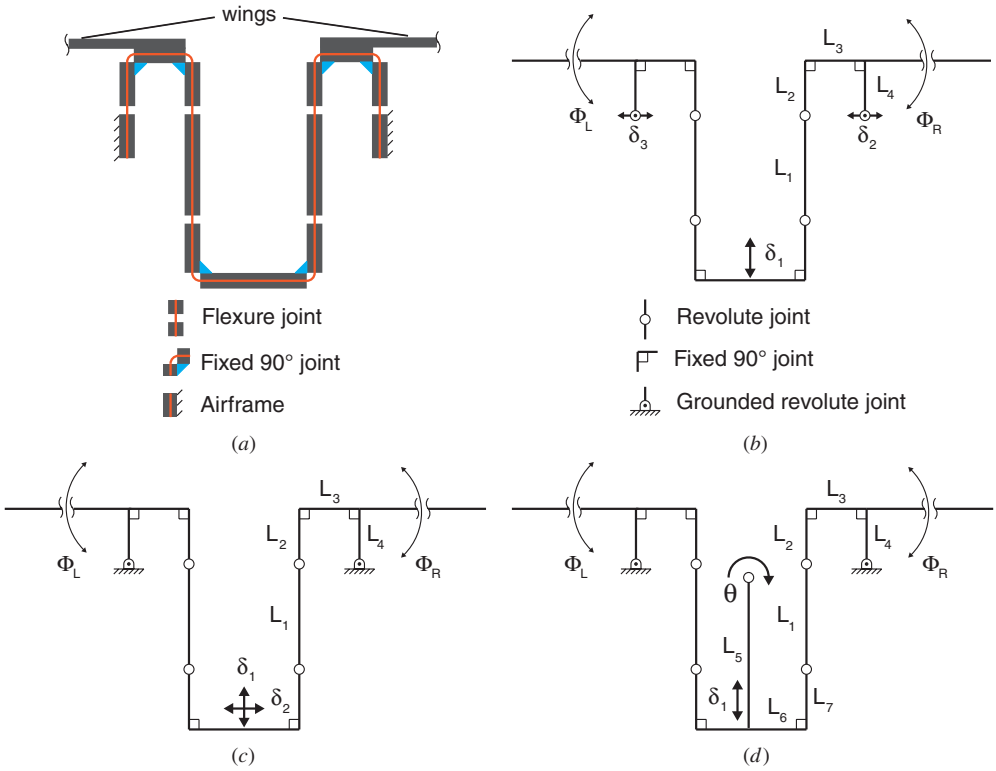

Figure 4. (*a*) A planar view of the flexure-based transmission mechanism, which converts actuator input motion to wing flapping motion. Use of a pseudo-rigid body model, where flexure joints are modeled as ideal revolute joints and all connecting spars are assumed to be rigid, allows geometric analysis of the transmission motion. Equivalent pseudo-rigid body models are shown for (*b*) design 1 with separate power and control actuators, (*c*) design 2 with a hybrid power-control actuator (two linear inputs) and (*d*) design 3 with one linear and one rotational input.

with subscripts L and R indicating the right and left wings, respectively.

(i) For design 1 (separate power and control actuators)

$$\mathrm{d}x_R = \delta_2 \tag{6}$$
$$\mathrm{d}x_L = \delta_3 \tag{7}$$
$$\mathrm{d}y_R \equiv 0 \tag{8}$$
$$\mathrm{d}y_L \equiv 0. \tag{9}$$

(ii) For design 2 (hybrid power-control actuator with two linear inputs)

$$\mathrm{d}x_R = -\delta_2 \tag{10}$$
$$\mathrm{d}x_L = \delta_2 \tag{11}$$
$$\mathrm{d}y_R \equiv 0 \tag{12}$$
$$\mathrm{d}y_L \equiv 0. \tag{13}$$

(iii) For design 3 (hybrid power-control actuator with one linear and one rotational input)

$$\mathrm{d}x_R = L_5 \sin\theta + L_6(\cos\theta - 1) - L_7 \sin\theta \tag{14}$$
$$\mathrm{d}y_R = L_5(\cos\theta - 1) - L_6 \sin\theta + L_7(1 - \cos\theta) \tag{15}$$
$$\mathrm{d}x_L = -\mathrm{d}x_R \tag{16}$$
$$\mathrm{d}y_L = -\mathrm{d}y_R. \tag{17}$$

The transmission kinematics can be used to compare how the three different designs can modulate stroke amplitude with control actuator motion, for a fixed power actuator input of $\pm 200\,\mu$m, and this is shown in figure 5. We see that designs 1 and 2 are kinematically equivalent and achieve the same change in stroke amplitude for a given control actuator displacement, the only difference being the reversal of the sign convention for δ_2. In both cases, the change in amplitude is fairly linear with control actuator displacement. We see that the third design, with a twisting actuator, has a much less linear response (note the trigonometric relationships for dx and dy in equations (14) and (15)) and does not achieve as large an amplitude change. We also note that, in practice, a unipolar drive signal must be used for the twisting unimorphs in order to avoid depoling the piezoelectric material. This means that only a positive *or* negative control actuator rotation can be used, not both. However, design 3 cannot be compared directly to designs 1 and 2 on a purely kinematic basis since the actuator input types are different (translational versus rotational).

3.2. Dynamics

A dynamic model of the system accounts for actuators as force, not displacement sources, and also includes non-geometric components such as wing inertia and aerodynamic loading (refer to figure 6 for relevant forces and inertias).

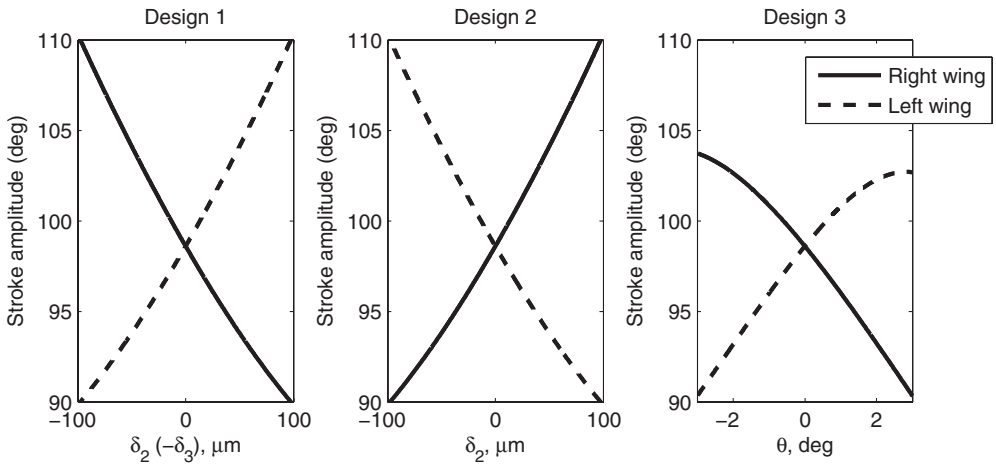

Figure 5. Stroke amplitude for the left and right wings over the range of control actuator motion with a fixed power actuator input of $\pm 200\,\mu$m, for each design.

The actuator–transmission–wing mechanism forms a spring–mass–damper system where the applied actuator force (and resulting displacement) is mapped to wing displacement through the nonlinear transmission kinematics (equation (1)), and aerodynamic wing loading serves as a nonlinear damping force (figure 6(*c*)). The differential equations governing the behavior of this system can be derived using an Euler–Lagrange energy formulation:

$$\frac{\mathrm{d}}{\mathrm{d}t}\left(\frac{\partial L}{\partial \dot{q}}\right) - \frac{\partial L}{\partial q} = \frac{\partial W_{\text{ext}}}{\partial q} \tag{18}$$

where L is the difference between kinetic and potential energy, q is a generalized coordinate vector whose size is equal to the number of DOFs of the system (the two coordinate spaces, actuator and wing, are related explicitly by the transmission kinematics and thus either can be chosen for convenience) and W_{ext} is the work done on the system by internal (actuation) and external (e.g. aerodynamic) forces. Use of this formulation therefore requires that all potential/kinetic energy and work terms be written as functions of the state variables q and time. Our model includes the following terms.

- Applied actuator force: a function of actuator geometry and applied electric field.
- Actuator elasticity: a function of actuator geometry and material properties.
- Wing inertia: a function of wing geometry and material properties.
- Aerodynamic damping: a function of wing profile, wing flapping velocity and angle of attack.

To simplify the model, we neglect actuator damping and inertia as these terms are small relative to those of the wing, and also neglect transmission dynamics for the same reason [5].

Starting with the power actuator, we have the applied actuator force (which can be any function, typically the system is driven with a harmonic drive for efficiency) and the spring force due to elastic deformation of the actuator:

$$F_{\text{act}} = F_0 \sin(2\pi f t) \tag{19}$$

$$F_{\text{spring}} = -k_{\text{act}}\delta \tag{20}$$

where F_0 is the peak actuator force, f is the actuator drive frequency, k_{act} is the actuator's equivalent linear spring constant and δ is the actuator tip displacement. A similar formulation can be used for the control actuator, or the control actuator can be treated as a kinematic input if its actuation frequency is low relative to the power actuator (i.e. its motion is quasi-static) and it is sufficiently stiff. Treating the wing as a beam, the kinetic energy of the flapping mode is given by

$$\text{KE}_{\text{wing}} = \tfrac{1}{2} J_{\text{wing}} \dot{\phi}^2 \tag{21}$$

where $\dot{\phi}$ is the rotational velocity and J_{wing} is the wing's inertia about the point of rotation. Aerodynamic forces are written as functions of wing geometry, angle-of-attack-dependent coefficients and flapping velocity, using a quasi-steady blade-element aerodynamic model [30]:

$$F_N = C_G C_N(\alpha)\dot{\phi}^2 \tag{22}$$

$$F_T = C_G C_T(\alpha)\dot{\phi}^2 \tag{23}$$

where F_N and F_T are the normal and tangential forces on the wing, C_G is a constant dependent on wing geometry and C_N and C_T are the normal and tangential force coefficients (which are empirically derived functions of the angle of attack α, see [18]). Note that aerodynamic forces are proportional to wing velocity squared. If stroke amplitude is increased while flapping frequency is held constant, this necessitates an increase in the flapping velocity of the wing. Thus, to first order, we expect an increase in stroke amplitude at constant frequency to lead to higher aerodynamic forces. Therefore if stroke amplitude can be controlled asymmetrically, asymmetric aerodynamic forces can be generated on the two wings, leading to net body torque and rotational motion (this is consistent with wing motion asymmetries measured during saccades in [1]). The present work, based on this first-order assumption, focuses on detailed modeling and measurement wing kinematics and not aerodynamic torques. Future work will encompass modeling

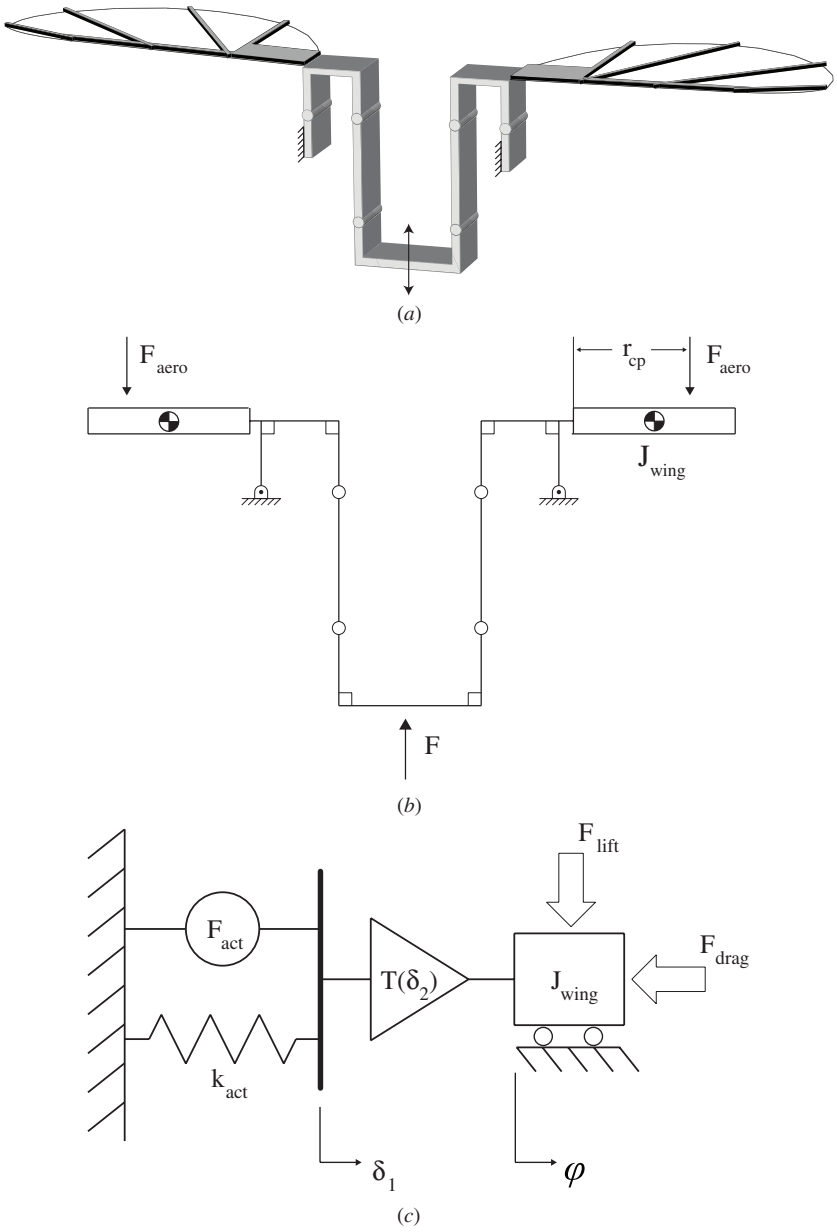

Figure 6. (*a*) The actuator serves as an oscillatory input to the central link of a symmetric fourbar transmission, which drives flapping motion of both the wings. (*b*) The system can be approximated by a planar pseudo-rigid body model where the actuator is loaded by both wing inertia and aerodynamic drag. (*c*) A lumped-parameter model treats the actuator as a force source in parallel with a linear spring, driving wing motion through a kinematically determined transmission ratio T which is a function of δ_2 (or θ).

and measurement of aerodynamic torques to validate this assumption.

Wing rotation about the longitudinal axis is passive and driven by aerodynamic and inertial forces [5]. For a typically observed wing trajectory, it is seen that the angle of attack is approximately 45° at the midestroke and 90° at the stroke reversals. Assuming that small variations in the stroke amplitude will not have a large effect on the nominal angle of attack trajectory, this can be expressed mathematically as

$$\alpha = \frac{\pi}{2} - \frac{\pi}{4}\cos\left(\sin^{-1}\left(\frac{\phi}{\phi_{\max}}\right)\right). \tag{24}$$

The normal and tangential forces are then transformed into drag and lift components, which act parallel to and perpendicular to the stroke plane respectively. The aerodynamic drag therefore acts as a damping force against the actuator, and is included in the energy formulation. Note that the aerodynamic force acts at the center of pressure of the wing, defined as a distance r_{cp} from the point of rotation. Thus the aerodynamic drag torque on the wing is expressed as

$$\tau_{\text{drag}} = F_{\text{drag}} r_{\text{cp}} \tag{25}$$

Using equations (19) through (25), the Euler Lagrange formulation can be evaluated to a second-order scalar ODE in ϕ:

$$J_{\text{wing}}\ddot{\phi} + \frac{k_{\text{act}}}{T^2}\phi = \tau_{\text{aero}} + \tau_{\text{act}} \tag{26}$$

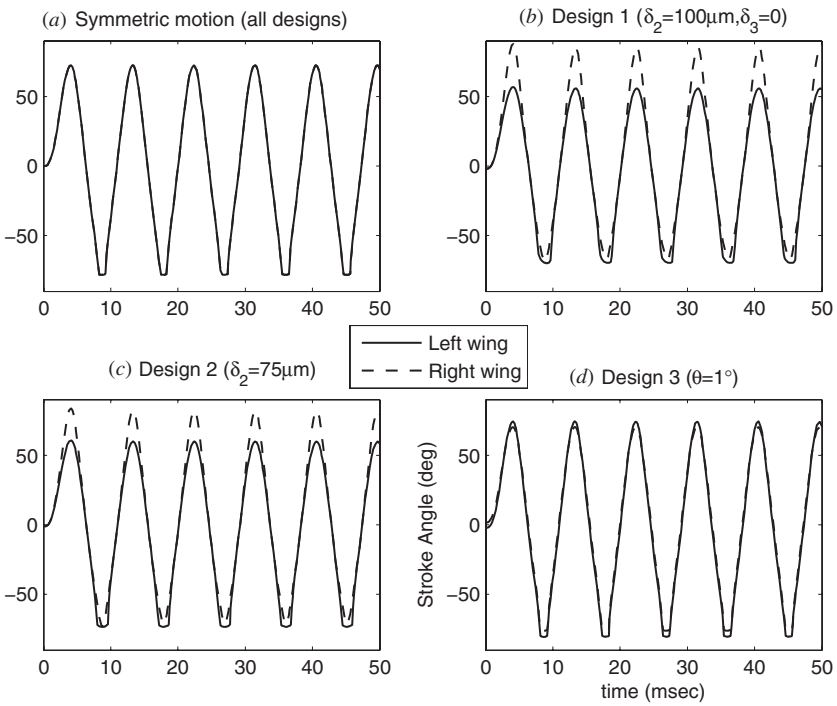

Figure 7. Stroke angle versus time solved numerically for each design. (*a*) Since the kinematics of each design are equivalent if the control actuator position(s) are zero (i.e. $\delta_2 = \delta_3 = \theta \equiv 0$), all three designs will exhibit bilaterally symmetric wing motion and thus no net body torque. For (*b*) design 1, (*c*) design 2 and (*d*) design 3, we see that a constant nonzero control actuator position with a sinusoidal power actuator input results in asymmetric stroke trajectories, with large asymmetries in stroke amplitude (generating a yaw torque) and small coupled changes in the mean stroke angle (which will lead to a small but coupled pitch torque). Note that the flapping motion is not perfectly symmetric about $\phi = 0$ since the transmission kinematics are nonlinear (equation (1)).

where T is the *transmission ratio*, defined as

$$T = \frac{\mathrm{d}\phi}{\mathrm{d}\delta_1} \tag{27}$$

which can be calculated with equation (1). The torque terms are defined as

$$\tau_{\text{aero}} = -F_{\text{drag}} r_{cp} \operatorname{sgn}(\dot{\phi}) \tag{28}$$

and

$$\tau_{\text{act}} = \frac{1}{T} F_{\text{act}}. \tag{29}$$

The $\operatorname{sgn}(\dot{\phi})$ term is required since, by convention, the drag force is always positive.

Equation (26) can be solved numerically to yield wing trajectories resulting from given actuator inputs. These trajectories are shown in figure 7 for each design. The reader is referred to [26, 27] for further details of this analysis; [31] also presents a thorough analysis of a 2DOF flapping-wing robotic system using an Euler–Lagrange formulation.

3.3. A note on model accuracy

Both kinematic and dynamic models are very sensitive to actuator parameters: peak displacement $\delta_{\max}$ for the kinematic model, peak force F_0 and spring constant k_{act} in the dynamic model. Actuator modeling and testing in [22, 28], while capable of predicting general performance trends based on actuator geometry, have shown errors of up to 30% between predicted and measured values, and performance ranges up to ±15% for actuators with the same geometry. As such, we do not rely too heavily on the models to exactly predict device performance. Rather, we use these models as guidelines to aid in designing transmission schemes that are able to generate controllable asymmetric stroke amplitudes, and then verify these designs experimentally. These experiments are discussed in the next section.

4. Materials and methods

Test structures were constructed to evaluate all three of the distributed actuation concepts, using a fabrication paradigm previously developed to address the difficulties in fabricating micro-scale robotic devices [29]. Test articles were fabricated with fiber-reinforced composites as structural elements (M60J carbon fiber and S2 glass fiber from Toray America, pre-impregnated with RS-3C resin from YLA Inc.), thin polymer films as flexure joints and wing membranes (Kapton polyimide and ultra-polyester from Chemplex Industries) and piezoelectric ceramics for actuation (PZT-5H from Piezo Systems Inc.) (figure 8). Piezoelectric actuators were driven with a custom control program written in Matlab (Mathworks Inc.), which sent drive signals to a digital-to-analog converter board (Q8 AD/DA board from Quanser Consulting). Analog output voltage from this board was increased to levels required to drive piezoelectric actuators (∼200 V) with a high voltage amplifier (Trek, Inc.). Test structures for all three designs are shown in figure 9.

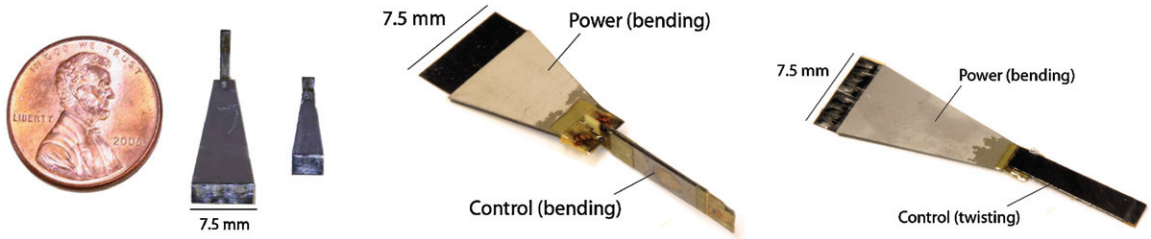

(*a*) (*b*) (*c*)

Figure 8. (*a*) Power actuator (large) and control actuator (small) used for design 1; (*b*) hybrid bending actuator used for design 2; (*c*) hybrid bending-twisting actuator used for design 3.

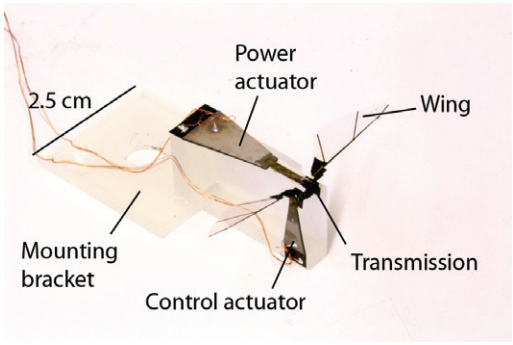

(*a*)

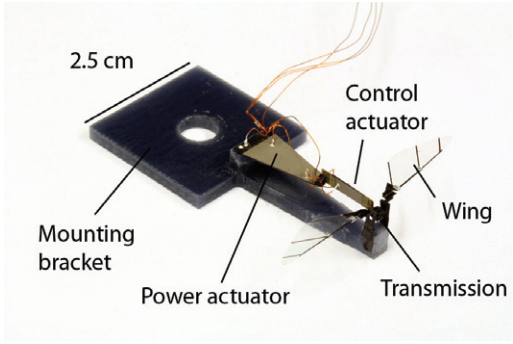

(*b*)

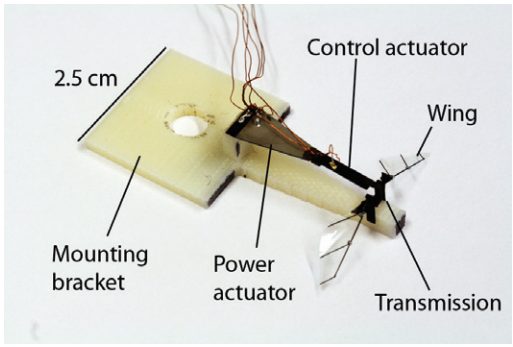

(*c*)

Figure 9. (*a*) Design 1: separate power and control actuators. Each actuator is a bending bimorph. (*b*) Design 2: hybrid power-control actuator. Each individual actuator is still a bimorph, but now a hybrid actuator is fabricated monolithically to allow 2DOF actuator motion. (*c*) Design 3: again a hybrid power-control actuation scheme, now with a bending bimorph for power and a twisting unimorph for control.

Videos to collect wing trajectory data were recorded with a Cooke pco.1200 hs high-speed camera at approximately 1600 frames s^{-1}. Initially, wing trajectories were digitized manually with a custom Matlab script. In order to increase the volume of data that could be collected, retroreflective markers (U92 tape from Reflexite Inc.) were placed on the leading edge of the wings, and automated 2D motion tracking software (ProAnalyst from Xcitex Inc.) was used to automatically track wing motion. Power actuator size was increased relative to the original HMF design in order to compensate for the increased wing inertia resulting from the addition of markers.

For each device, the single-power actuator was driven at the flapping resonant frequency (verified empirically after initial predictions by dynamic modeling) and stroke amplitudes were recorded over a range of control actuator motion, in order to determine if the predicted changes in stroke amplitude could be observed. Changes in the angle of attack during the stroke, while expected as a second order effect, were not recorded since our designs focus primarily on modulation of stroke amplitude.

5. Results

We recorded the range of stroke amplitudes over the full range of control actuator motion for each of the three devices. Overlaid frames from videos of design 1 are presented in figure 10, illustrating the asymmetric changes in stroke amplitude. Recorded wing trajectories as a function of time for all three designs, at opposite extremes of control actuator motion, are shown in figure 11. Experimentally recorded bilateral asymmetries in stroke amplitude are summarized in table 1 and compared to values predicted using the modeling in section 3 (for more detailed experimental data for designs 1 and 2, see [26, 27]). As predicted by kinematic and dynamic analyses, each individual design is capable of causing changes in stroke amplitude through motion of the smaller control actuators, while holding the driving motion of the larger power actuators fixed. Furthermore, each design produces bilateral asymmetries in stroke amplitude of similar magnitude observed in Diptera during rapid saccades [1]. Note that there are also inherently coupled changes in the mean stroke angle in the experimental devices, which may result in coupling with torques about other body axes (i.e. pitch and roll instead of yaw). However, the transmission geometry can be optimized to maximize changes in stroke amplitude while minimizing changes in the mean stroke angle, effectively decoupling torques about the three principal body axes.

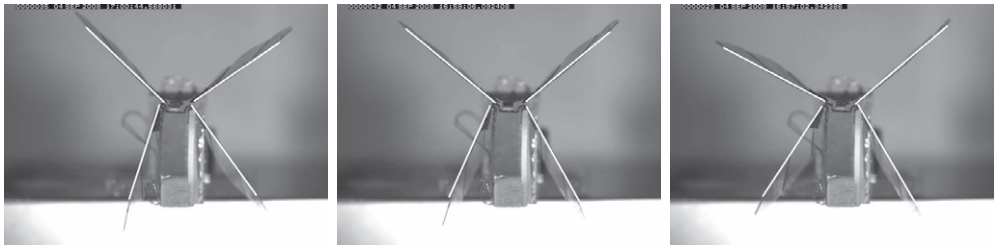

(*a*) (*b*) (*c*)

Figure 10. Overlaid frames from three different flapping videos of design 1 with separate power and control actuation. The power actuator input is the same for each video, but control actuator motion is swept from left to right extremes, resulting in stroke amplitude asymmetry. The leading edges of the wings are highlighted with a white line in each frame for clarity. In (*a*) the stroke amplitude of the left wing is greater than that of the right wing, in (*b*) the amplitudes are approximately equal and in (*c*) the amplitude of the left wing is smaller. Note that only the left wing is attached to a control actuator and thus experiences an amplitude change; the right wing pivot is connected to the ground and thus its amplitude stays roughly constant.

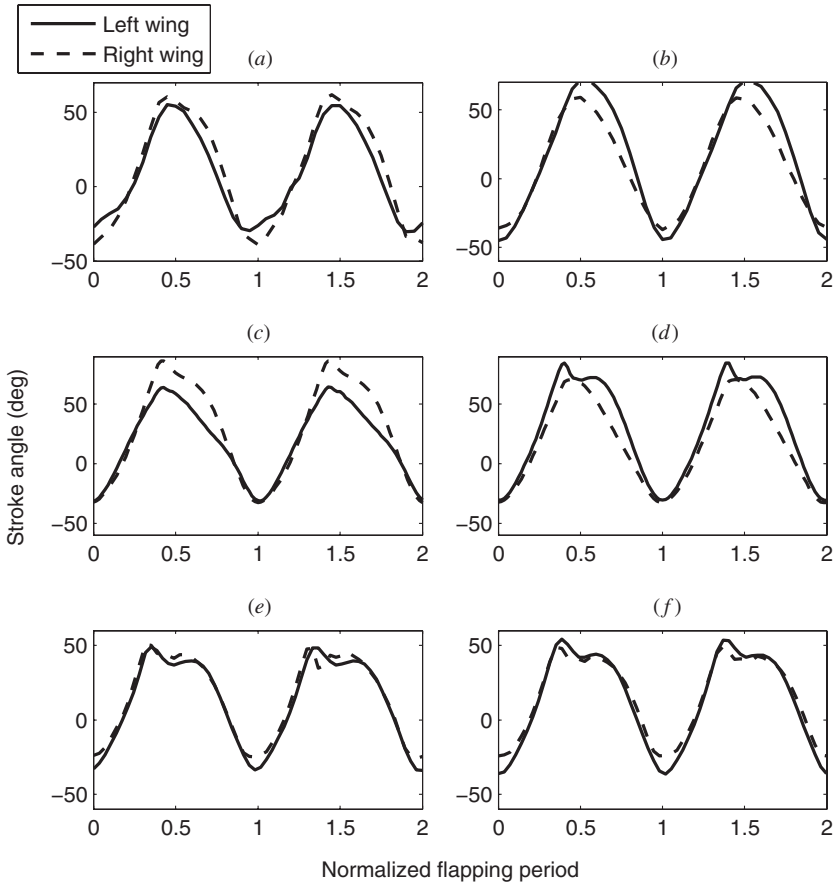

Figure 11. Recorded wing stroke angles for the left and right wings for each of the three different designs, at both extremes of control actuator motion. (*a, b*) design 1, (*c, d*) design 2 and (*e, f*) design 3. Flapping frequencies are 80 Hz, 35 Hz and 50 Hz respectively for the three designs (due to different resonant frequencies of the experimental devices). The power actuator input is held constant for each test (200V drive signal), showing that the resulting change in stroke amplitude is due to control actuator motion.

Our previous two designs [26, 27] were not initially compared based on any common criteria. A universal metric must be selected to compare all three designs in order to evaluate which is the most effective at performing the ultimate goal of generating a yaw torque. Final vehicle designs must take into account tradeoffs between maneuverability and stability, the mass of control actuators (thus their impact on the overall weight budget and flight time) and the power consumption required for a given maneuver. This design optimization may be aided by examining evolutionary pressures on flying insects relative to mission requirements for MAVs. For example, while increased maneuverability can aid in evading predators and obstacles or be useful in aerial courtship, these rapid accelerations require exertion of additional mechanical power, and flight strategies that minimize energy expenditure per unit *distance* (thus to maximize distance traveled with given amount of energy) may differ from strategies to minimize energy per unit *time* (thus to

Table 1. Bilateral asymmetries in stroke amplitude. For each design, kinematic and dynamic predictions are compared to experimentally observed stroke amplitude asymmetries for a given control actuator displacement. Note that the test device used for design 1 only had one control actuator (figure 9(*a*)), not two as shown in figure 3, so $\delta_3 = 0$ for the simulations in order to be consistent with experiments.

Device	δ_2 or θ	Kinematic	Dynamic	Measured
Design 1	100 μm	12°	27°	18°
Design 2	75 μm	16°	20°	35°
Design 3	1°	4°	8°	17°

Table 2. Percentage difference in stroke amplitude, control actuator mass and performance metric R for each design.

Device	$\Delta\phi_{\text{tot}}$	m_{act}	R
Device 1	21%	41 mg	0.51
Device 2	23%	19 mg	1.2
Device 3	23%	19 mg	1.2

stay aloft as long as possible) [2]. While it would be premature to select the 'best' design since currently only kinematic data for wing trajectories are available (as opposed to actual torque data or rotational velocity/acceleration data from a vehicle actually capable of controlled turns), we can define a simple performance metric based on the data presented here. Each of the three designs presented has the same goal: produce a bilateral stroke amplitude asymmetry. Since each design uses the same power actuator but a different control actuator, we define the performance metric R as the ratio of *bilateral difference in stroke amplitudes* to *control actuator mass*. We use the percentage difference in stroke amplitudes rather than absolute values, since the peak-to-peak amplitude was not necessarily the same for each device. Thus we have

$$R = \frac{\Delta\phi_{\text{tot}}(\%)}{m_{\text{act}}} \tag{30}$$

where $\Delta\phi_{\text{tot}}$ is the amplitude difference between the left and right wings expressed as a percentage, and m_{act} is the control actuator mass. These values are presented in table 2 for each design. We see that, despite having a smaller absolute value for stroke amplitude difference, design 3 actually has the same percentage difference in stroke amplitude as design 2, since the total amplitudes are smaller (see table 1 and figure 11). Thus, since the control actuator masses are the same, the two designs have the same value of R. Design 1, despite having a similar $\Delta\phi_{\text{tot}}$, has a much heavier control actuator and therefore a smaller value of R. However, we cannot eliminate design 1 as a viable candidate for an autonomous vehicle based on this very preliminary analysis without further experimental data, including actuator power consumption and torque measurements.

6. Conclusions and future work

These designs demonstrate that, through the use of mechanical design, actuation and fabrication techniques developed to address the issue of creating mobile insect-scale robots, biologically inspired insect wing motions can be mechanically recreated in an at-scale device. The distribution of power and control actuators in the thoracic mechanics of actual insects serves as an inspiration for designs capable of reproducing asymmetric wing stroke amplitudes as observed in yawing maneuvers of dipteran insects. While a quasi-steady aerodynamic model predicts that such differential control of stroke amplitude will lead to controlled yaw torques, this work only considers kinematic motion of the wings. Experimental validation of the ability to generate torques is essential to confirm this prediction and develop control laws for stabilization and trajectory following. Further understanding of how wing kinematics map to net body torques and how insects use these motions for stabilization and maneuvering will help lead to the ultimate goal of an autonomous, freely flying vehicle.

Acknowledgments

This work was supported in part by the Army Research Laboratory (award number W911NF-08-2-0004), the National Science Foundation (award number CMMI-07466 38) and by the Department of Defense (DoD) through the National Defense Science & Engineering Graduate Fellowship (NDSEG) Program. Any opinions, findings and conclusions or recommendations expressed in this material are those of the authors and do not necessarily reflect those of the National Science Foundation. The authors also thank Pierre Duhamel for artistic help with figure 3.

References

[1] Fry S N and Dickinson M H 2003 The aerodynamics of free-flight maneuvers in *Drosophila Science* **300** 495–8
[2] Dudley R 2000 *The Biomechanics of Insect Flight: Form, Function, Evolution* (Princeton, NJ: Princeton University Press)
[3] Fearing R, Chiang K H, Dickinson M H, Pick D L, Sitti M and Yan J 2000 Wing transmission for a micromechanical flying insect *IEEE Int. Conf. on Robotics and Automation* vol 2 pp 1509–16
[4] Wood R J 2007 Liftoff of a 60 mg flapping-wing MAV *IEEE/RSJ Int. Conf. on Intelligent Robots and Systems* pp 1889–94
[5] Wood R J Design, fabrication and analysis, of a 3DOF, 3 cm flapping-wing MAV *IEEE/RSJ Int. Conf. on Intelligent Robots and Systems* pp 1576–81
[6] Wood R J 2008 The first takeoff of a biologically inspired at-scale robotic insect *IEEE Trans. Robot.* **24** 341–7
[7] Williams C M and Williams M V 1943 The flight muscles of *Drosophila repleta. J. Morphol.* **72** 589–99
[8] Vigoreaux J O 2006 *Nature's Versatile Engine: Insect Flight Muscle Inside and Out* (Berlin: Springer)
[9] M S Tu and Dickinson M H 1996 The control of wing kinematics by two steering muscles of the blowfly *Calliphora vicina. J. Comp. Physiol.* A **178** 813–30
[10] Tu M and Dickinson M 1994 Modulation of negative work output from a steering muscle of the blowfly *Calliphora vicina. J. Exp. Biol.* **192** 207–24
[11] Taylor G K 2001 Mechanics and aerodynamics of insect flight control *Biol. Rev. Camb. Philos. Soc.* **76** 449–71
[12] Taylor G K 2005 Flight muscles and flight dynamics: towards an integrative framework *Animal Biol.* **55** 81–99

[13] Ellington C P 1999 The novel aerodynamics of insect flight: applications to micro-air vehicles *J. Exp. Biol.* **202** 3439–48
[14] Zanker J M 1988 How does lateral abdomen deflection contribute to flight control of *Drosophila melanogaster*? *J. Comp. Physiol.* A **162** 581–8
[15] Combes S A 2010 Personal communication
[16] Dudley R 2002 Mechanisms and implications of animal flight maneuverability *Integr. Comp. Biol.* **42** 135–40
[17] Bergou A J, Xu S and Wang Z J 2007 Passive wing pitch reversal in insect flight *J. Fluid Mech.* **591** 321–37
[18] Dickinson M, Lehmann F and Sane S P 1999 Wing rotation and the aerodynamic basis of insect flight *Science* **284** 1954–60
[19] Sitti M 2001 PZT actuated four-bar mechanism with two flexible links for micromechanical flying insect thorax *IEEE Int. Conf. on Robotics and Automation* vol 4 pp 3893–900
[20] Avadhanula S, Wood R J, Campolo D and Fearing R S 2002 Dynamically tuned design of the MFI thorax *IEEE Int. Conf. on Robotics and Automation* vol 1 pp 52–9
[21] Sreetharan P S and Wood R J 2010 Passive aerodynamic drag balancing in a flapping-wing robotic insect *J. Mech. Design* **132** 051006
[22] Wood R J, Steltz E and Fearing R S 2005 Optimal energy density piezoelectric bending actuators *Sensors Actuators* A **119** 476–88
[23] Karpelson M, Wei G Y and Wood R J 2009 Milligram-scale high-voltage power electronics for piezoelectric microrobots *IEEE Int. Conf. on Robotics and Automation*
[24] Marden J H 1987 Maximum lift production during takeoff in flying animals *J. Exp. Biol.* **130** 235
[25] Karpelson M, Whitney P, Wei G Y and Wood R J 2010 Energetics of flapping-wing robotic insects: towards autonomous hovering flight *IEEE/RSJ Int. Conf. on Intelligent Robots and Systems* under review
[26] Finio B, Shang J and Wood R J 2009 Body torque modulation for a microrobotic fly *IEEE Int. Conf. on Robotics and Automation* pp 3449–56
[27] Finio B, Oland C, Eum R J and Wood B 2009 Asymmetric flapping for a robotic fly using a hybrid power-control actuator *IEEE/RSJ Int. Conf. on Intelligent Robots and Systems*
[28] Finio B and Wood R J 2010 Optimal energy density piezoelectric twisting actuators *Sensors Actuators* A under review
[29] Wood R J, Avadhanula S, Sahai R, Steltz E and Fearing R S 2008 Microrobot design using fiber reinforced composites *J. Mech. Design* **130** 52304–15
[30] Whitney J P 2010 Aeromechanics of passive rotation in flapping flight *J. Fluid Mech.* at press
[31] Avadhanula S 2006 Design, fabrication and control of the micromechanical flying insect *PhD Thesis* University of California, Berkeley